Taylor & Francis
Taylor & Francis Group

Journal of Macromolecular Science, Part A
Pure and Applied Chemistry

ISSN: 1060-1325 (Print) 1520-5738 (Online) Journal homepage: www.tandfonline.com/journals/lmsa20

Gemcitabine-loaded Ca^{2+}-crosslinked high-amylose starch beads as intratumoral depot candidates: microporosity, release, and *in vitro* activity

Hakan Avcı, Deniz Ceylan & Nil Azra Aytekin

To cite this article: Hakan Avcı, Deniz Ceylan & Nil Azra Aytekin (2025) Gemcitabine-loaded Ca^{2+}-crosslinked high-amylose starch beads as intratumoral depot candidates: microporosity, release, and *in vitro* activity, Journal of Macromolecular Science, Part A, 62:12, 1359-1370, DOI: 10.1080/10601325.2025.2586576

To link to this article: https://doi.org/10.1080/10601325.2025.2586576

JOURNAL OF MACROMOLECULAR SCIENCE, PART A: PURE AND APPLIED CHEMISTRY
2025, VOL. 62, NO. 12, 1359–1370
https://doi.org/10.1080/10601325.2025.2586576

Gemcitabine-loaded Ca^{2+}-crosslinked high-amylose starch beads as intratumoral depot candidates: microporosity, release, and *in vitro* activity

Hakan Avci[a,b,c], Deniz Ceylan[d], and Nil Azra Aytekin[b]

[a]Faculty of Pharmacy, Departmant of Pharmaceutical Technology, Istanbul University, Istanbul, Turkey; [b]Faculty of Pharmacy, Bezmialem Vakif University, Istanbul, Turkey; [c]Faculty of Arts and Sciences, Physics, Yildiz Technical University, Istanbul, Turkey; [d]Pharmaceutical Biotechnology, Bezmialem Vakif University, Istanbul, Turkey

ABSTRACT

Pancreatic ductal adenocarcinoma (PDAC) motivates localized drug-delivery strategies that increase intratumoral exposure while limiting systemic toxicity. Here, we report spherical high-amylose starch beads prepared by droplet gelation and Ca^{2+} ionotropic crosslinking as a simple, water-based depot platform. The beads preserved spherical geometry and displayed an interconnected microporous interior by SEM. FTIR supported Ca^{2+}-OH interactions within the starch network and non-covalent (physical) loading of gemcitabine without evidence of new covalent bonds. In PBS (pH 6.6, 37 °C), formulations with 10–15% $CaCl_2$ maintained structural integrity yet underwent enzyme-responsive erosion in α-amylase (≈ 8–10 days), suggesting residence times compatible with intratumoral depots. HPLC-UV enabled quantification of gemcitabine encapsulation efficiency (EE = 4.14%), corresponding to ~3.53 µg per bead (30 beads analyzed). *In vitro* release under sink conditions exhibited a burst-to-plateau profile with near-quantitative mass recovery (≈100% of the loaded dose within hours). Preliminary cell studies were performed with PANC-1 to assess functional delivery. Collectively, these data indicate that Ca^{2+}-crosslinked starch beads are *in vitro* tolerable, solvent-free, and injection-ready candidates for intratumoral chemotherapy. Limitations include the modest EE and rapid early release; avenues to address these (e.g., network densification or secondary coatings and process optimization) are outlined, together with the need for *in vivo* evaluation of residence, pharmacokinetics, and safety.

GRAPHICAL ABSTRACT

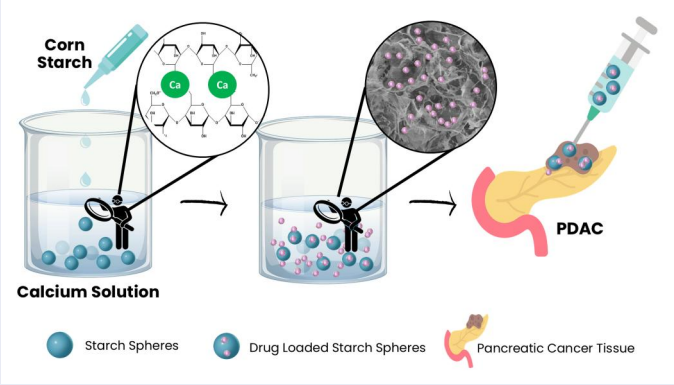

ARTICLE HISTORY
Received October 2025
Accepted November 2025

KEYWORDS
High-amylose starch; ionotropic gelation; calcium crosslinking; intratumoral depot; gemcitabine; pancreatic cancer

1. Introduction

Pancreatic ductal adenocarcinoma (PDAC) remains among the most lethal solid tumors: in contemporary U.S. datasets only ~13% of patients are alive at 5 years, and over half present with distant disease at diagnosis, underscoring the need for more effective locoregional strategies.[1] Systemic gemcitabine-a longstanding backbone therapy-suffers from rapid plasma inactivation *via* cytidine deaminase and short half-life, which limits intratumoral exposure while systemic dosing drives toxicity.[2] Beyond pharmacokinetics, PDAC's dense, hypovascular, desmoplastic stroma acts as a physical and physiological barrier that impedes perfusion and drug penetration, contributing to chemoresistance.[3] These limitations have motivated locoregional and intratumoral drug-delivery approaches—often under endoscopic ultrasound (EUS) guidance—to augment tumor drug levels while minimizing systemic exposure. Early clinical studies have shown that EUS-

CONTACT Deniz Ceylan deniz.ceylan@bezmialem.edu.tr Faculty of Pharmacy, Bezmialem Vakif University, 34093 Istanbul, Turkey.
Supplemental data for this article can be accessed online at https://doi.org/10.1080/10601325.2025.2586576.

guided fine-needle injection (FNI) of agents, including gemcitabine, is feasible and safe, supporting the broader exploration of injectable depots for PDAC.[4]

Biopolymer hydrogels are the attractive candidates for such depots due to their injectability, tunable mesh size, and biodegradability. Starch, in particular, is abundant, inexpensive, and *in vitro* tolerable; high-amylose grades form stronger, more ordered networks and can degrade enzymatically (e.g., α-amylase-mediated hydrolysis), features that make starch matrices promising for controlled drug release.[5] In the pancreas, α-amylase is produced at high concentrations in exocrine secretions, providing a clinically relevant enzymatic milieu that can enable the controlled degradation of starch-based depots after local therapy.[6]

Ionotropic gelation with multivalent cations—classically Ca^{2+} with alginate—is a simple, water-based crosslinking route that yields mechanically stable, injectable hydrogels and beads; similar ion-mediated strategies have also been reported for other polysaccharides (e.g., gellan).[7,8] For starch, most prior drug-delivery microspheres/hydrogels rely on chemical crosslinkers such as epichlorohydrin, sodium trimetaphosphate (STMP), or citric acid, or on physical gelation *via* gelatinization/retrogradation; nonetheless, recent food/biomaterial studies indicate that $CaCl_2$ can modulate starch gelatinization/retrogradation and gel properties, suggesting an opportunity for ionically reinforced starch networks.[9–11]

Here, we introduce, to our knowledge, the first droplet-gelation synthesis of spherical, Ca^{2+}-crosslinked high-amylose starch beads engineered as intratumoral depots candidate for PDAC. We fabricate and physicochemically characterize the beads with scanning electron microscopy (SEM)-derived microporosity, Fourier-transform infrared spectroscopy (FTIR) signatures quantify swelling stability and α-amylase-driven degradation under the near-physiological conditions, assess mechanical handling properties, and evaluate gemcitabine loading, *in vitro* release under sink conditions, and preliminary activity on PANC-1 cells. By coupling a biodegradable, enzyme-responsive polysaccharide matrix with simple Ca^{2+} ionotropic crosslinking, this platform aims to enable the localized chemotherapy.

2. Methods

2.1. Materials

High amylose corn starch (HYLON VII, ~70% amylose content; 13% moisture; 2.06×10 g/mol molecular weight), sodium hydroxide (NaOH) (≥98%, Sigma-Aldrich), calcium chloride dihydrate (Merck), and distilled water were used for the synthesis of beads. α-amylase enzyme from *Aspergillus oryzae* was purchased from Sigma-Aldrich for use in enzyme sensitivity tests. Phosphate buffer (PBS) (Sigma-Aldrich) was used as a solubilization medium for α-amylase enzyme. Gemcitabine hydrochloride (≥97%, 1PlusChem) was used for high-performance liquid chromatography (HPLC) analysis, drug loading and releasing, and *in vitro* tests. Sodium dihydrogen phosphate (Riedel-de Haen) and methanol (Merck) were used to prepare mobile phase for HPLC analysis. pH adjustment of the phosphate buffer for HPLC was done with orthophosphoric acid (85%) (Carlo Erba Reagenti). Dimethyl sulfoxide (DMSO) was also used in *in vitro* experiments.

2.1. Synthesis of starch beads

Starch granules (Hylon VII; high-amylose corn starch) were dispersed in aqueous NaOH solutions (0.1–3% w/v; concentration specified per formulation in Table 1) and stirred at 70 °C for 15 min to obtain an ionized, gelatinized starch solution (Fig. 1). The solution was then allowed to stand at room temperature to stabilize the synthesis conditions.

Subsequently, the ionic starch solution was transferred to a syringe and delivered dropwise into a previously prepared $CaCl_2$ bath (5–20% w/v; Table 1) using a syringe pump, resulting in the formation of Ca^{2+}–starch complex beads. The beads were cured in the $CaCl_2$ solution for 24 h and then used in subsequent experiments. A syringe pump (New Era NE-1800) equipped with a 10 mL syringe (17 mm inner diameter) and a 21-gauge needle delivered the ionized starch solution at 10 μL·min^{-1}. The needle-to-bath distance was 10 cm. The $CaCl_2$ gelling bath volume was 25 mL, maintained at room temperature and without stirring during droplet formation.

2.2. Characterization of the beads

2.2.1. Structure analysis

FTIR spectra were acquired for native starch (Hylon VII powder), gemcitabine hydrochloride, blank beads (F2.2), and gemcitabine-loaded beads (F2.2) to confirm Ca^{2+}-mediated complexation and drug incorporation. Measurements were performed on a Bruker ALPHA FTIR spectrometer. Bead samples were lyophilized after synthesis and analyzed as dry solids. Spectral range was 4,000–400 cm^{-1}; resolution 4 cm^{-1} with 32 co-added scans per spectrum (background: 32 scans). Measurements were carried out at room temperature. Spectra were processed in OPUS. An air/background spectrum was collected prior to each sample run.

2.2.2. Morphological analysis (SEM)

After reaching swelling equilibrium, the lyophilized beads of F2.2 were mounted on aluminum stubs using carbon adhesive tape and sputter-coated with gold for 20 s. Imaging was performed on a JEOL SEM-7100-EDX at an accelerating voltage of 1 kV under high-vacuum conditions, using the secondary electron detector. For size analysis, beads were measured from using ImageJ after scale calibration.

2.2.3. Swelling tests

Swelling behavior of freshly prepared starch–Ca^{2+} beads was evaluated under different pH conditions. Their initial wet weights (m_0) were recorded at the beginning of the test. Three selected formulations (F2.1, F2.2, and F2.3) were immersed in buffer solutions of pH 3.0, pH 7.4 (PBS), and pH 8.0. Swelling measurements were conducted at

predetermined time intervals (0, 3, 6, 9, 24, 48, 72, 96, and 144 h). At each time point, beads were carefully removed from the buffer, blotted to remove excess surface liquid, weighed to obtain the swollen weight ($m\square$), and then immediately transferred into fresh buffer solution. Buffer replacement was performed at each measurement point to maintain stable swelling conditions and eliminate interference from dissolved components. All swelling experiments were performed in triplicate ($n = 3$).

The relative mass (MR) was calculated according to:

$$m_{rel} = \frac{m_t - m_0}{m_0}$$

where m_{rel} is the relative mass change m_0 is the initial wet weight of the beads after stabilization, and $m\square$ is the weight at time t.α-Amylase sensitivity tests:

Freshly prepared starch–Ca^{2+} beads (F2.1, F2.2, and F2.3) were used for enzymatic degradation studies. For each formulation, 20 beads were immersed in 15 mL of α-amylase solution (1 mg/mL in PBS) and incubated at 37 °C under cyclic shaking (90 rpm). Enzymatic sensitivity was assessed by sampling every 48 h, at which time the incubation medium was replaced with fresh α-amylase solution to maintain the enzyme activity.

Table 1. Preformulation study formulations used in the synthesis of starch beads. Different concentrations of starch (5–20% w/v) and $CaCl_2$ (5–20% w/v) were tested to evaluate their effect on bead formation, while NaOH concentration was kept at 0.1–3% w/v.

Formulation		Starch (% w/v)	NaOH (% w/v)	$CaCl_2$ (% w/v)
F1	F1.1	5	1	5
	F1.2			10
	F1.3			15
	F1.4			20
F2	F2.1	10	1	5
	F2.2			10
	F2.3			15
	F2.4			20
F3	F3.1	15	1	5
	F3.2			10
	F3.3			15
	F3.4			20
F4	F4.1	10	0.1	5
	F4.2		0.5	
	F4.3		2	
	F4.4		3	

2.3. Mechanical tests

Uniaxial compression tests were carried out on spherical starch gel samples using a texture analyzer (Stable Micro Systems, UK) equipped with a cylindrical probe operating at a constant speed of 1 mm/s. For statistical reliability, at least 10 beads from each formulation were tested, and the average values were reported. Because the contact area between a flat probe and a spherical hydrogel change continuously during compression, the conventional analysis methods used for cylindrical samples are not directly applicable. Instead, the Hertz contact theory was employed to calculate the apparent Young's modulus of the beads, which is widely used for spherical hydrogel and biopolymer systems.[12–14] According to this model, the force-deformation relationship is expressed as:

$$F = \frac{4}{3} G D^{1/2} \Delta D^{3/2}$$

where F is the applied force (N), G is the Young's modulus (Pa), D is the undeformed bead diameter (m), and ΔD is the deformation (m).

2.4. Quantification of gemcitabine by HPLC

Gemcitabine hydrochloride (GEM) concentrations were determined using a Shimadzu Prominence LC-20 high-performance liquid chromatography (HPLC) system equipped with a UV detector set at 270 nm. Separations were performed on a C18 column (250 × 4.6 mm, 5 µm) under the isocratic conditions. The mobile phase consisted of methanol and 10 mM sodium dihydrogen phosphate buffer (pH 3.5) at 40:60 (v/v), delivered at a flow rate of 1.0 mL min^{-1}.[15] The injection volume was 20 µL, and the column was operated at room temperature. All samples were filtered through 0.22-µm syringe filters prior to injection. The validated HPLC method was subsequently applied for determining

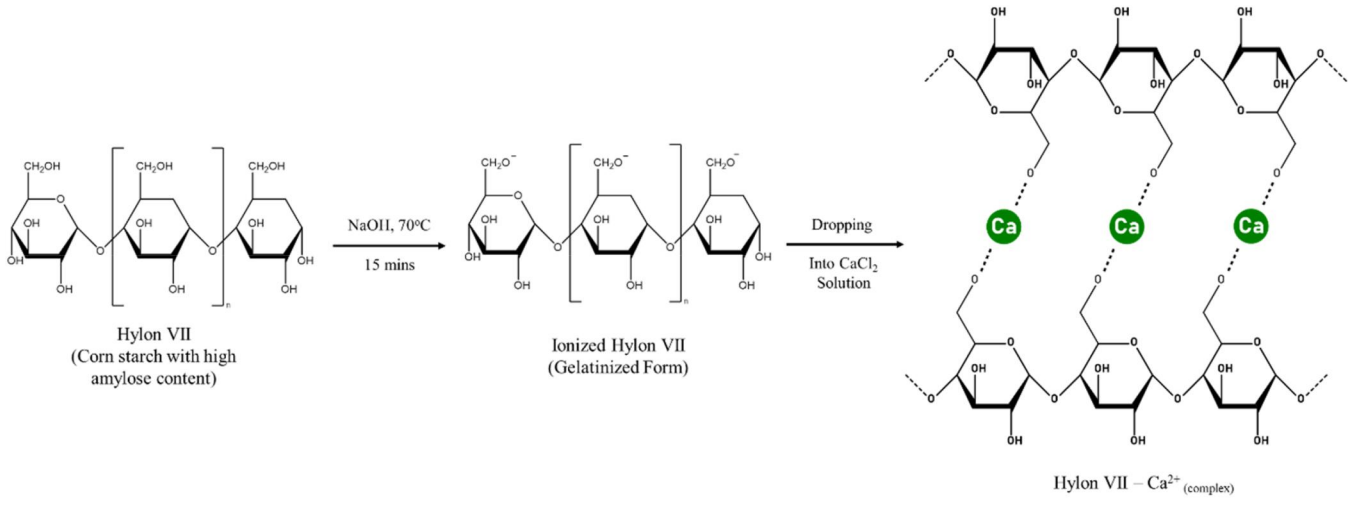

Figure 1. Stages of starch ionization and production of beads.

encapsulation efficiency and monitoring GEM release profiles.

2.5. Drug loading and encapsulation efficiency (EE)

For F2.2, the gelatinized ionic starch was cooled to room temperature, then reheated to 37 °C to reduce viscosity. Gemcitabine·HCl was added directly to obtain 5 mg mL^{-1}, mixed until dissolved, and cooled to room temperature, and 0.5 mL of the drug-containing feed was dispensed into the $CaCl_2$ bath (25 mL, RT, no stirring) with the syringe-pump settings described before (10 µL min^{-1}, 21 G, 10 cm). Approximately 30 beads formed and were cured for 24 h. After curing, supernatant aliquots were analyzed by HPLC:

$$\text{EE } (\%) = \frac{C_0 V_0 - C_s V_{\text{bath}}}{C_0 V_0} x\ 100$$

where C_0 is the initial concentration of gemcitabine in the feed solution, V_0 is the dispensed feed volume dropped into the $CaCl_2$ bath, C_s is the gemcitabine concentration measured in the curing supernatant, V_{bath} is the total volume of the $CaCl_2$ curing bath.

2.6. In vitro release

Release was assessed in PBS (pH 6.6) to mimic the mildly acidic tumor microenvironment. 30 beads ($n = 3$ batches) were placed in 15 mL medium at 37 °C and shaken at 90 rpm. About 1.0 mL of sample were withdrawn at 19 time points over 0–48 h and immediately replaced with fresh medium to maintain sink conditions. GEM concentrations were quantified by HPLC. Cumulative release (%) is calculated as:

$$m_i = VC_i + v\sum_{j=1}^{i-1} C_j \Rightarrow \%\text{Release}_i = \frac{m_i}{m_{\text{loaded}}} x100$$

where C_i is the concentration measured in the i-th sample, V is the total volume of release medium in the vessel, v is the aliquot volume withdrawn at each sampling, m_{loaded} is the initial amount of drug placed in the vessel, and m_i is the cumulative amount of drug released up to sampling time i.

2.6. In vitro efficacy tests

In vitro analyses were performed with human pancreatic cancer cell line (PANC-1). The viability of the cells was analyzed by MTT assay. Accordingly, the extraction medium was prepared according to ISO 10993-5:2009. PANC-1 cells were seeded in 24-well plates at 2×10^3 cells $well^{-1}$ and allowed to attach overnight at 37 °C, 5% CO_2. Drug-loaded and blank F2.2 beads were applied at a ratio of 1 bead per 0.3 mL of medium (Opti-MEM) and incubated for 24 h or 48 h at 37 °C. Cell viability was quantified by MTT. After exposure, cells were washed with PBS and treated with 50 µL MTT (5 mg mL^{-1} in PBS) plus 300 µL fresh Opti-MEM for 4 h at 37 °C. The medium was removed, the resulting formazan crystals were dissolved in 1 mL DMSO, and absorbance was read at 570 nm using a microplate reader (BioTek Synergy H1, USA). All experiments were performed in triplicate ($n = 3$). Cell viability (%) was calculated as:[16]

$$\text{Cell viability } (\%) = \frac{\text{OD of the experimental group}}{\text{OD of the control group}} x100$$

3. Results and discussion

3.1. Synthesis of starch beads

Bead formation depended sensitively on starch concentration, NaOH level during gelatinization, and the $CaCl_2$ concentration in the gelling bath. In alkaline dispersion, NaOH promotes starch swelling/gelatinization by disrupting hydrogen bonding and reducing short-range order; at higher alkali, partial chain scission and loss of crystallinity can occur (high-amylose corn starch, Hylon VII).[17] Moreover, Ca^{2+} interacts with starch hydroxyls and can physically crosslink/stabilize the gel network without creating new covalent bonds, which rationalizes the rapid setting of droplets in $CaCl_2$.[18]

Starch-specific bands are observed in spectra (Figure S4): broad O-H stretching (≈ 3,550–3,100 cm^{-1}), weak C-H stretching (≈ 2,930 cm^{-1}), H-O-H bending (≈ 1,640–1,650 cm^{-1}), and C-O/C-O-C vibrations in the fingerprint region (≈ 1,155–1,000 cm^{-1}). The slight redshift/intensity increase in the O-H band after cross-linking with Ca^{2+} and the changes in band intensities around 1,000–1,150 cm^{-1} can be attributed to the interaction between -OH groups and Ca^{2+} and stronger hydrogen bonds; similarly, the Ca^{2+}–starch interaction has been reported to be monitored by changes around the -OH area in FTIR. Additionally, the density ratio 1,047/1,022 cm^{-1} is used as an indicator of short-range order/crystallinity; higher amylose content tends to increase this ratio and is compatible with high-amylose Hylon VII system.[19]

In F1 initial droplets formed but stability was poor: After tens of additions, fresh droplets coalesced into aggregates and, in some formulations formed unstable materials that were not perfectly spherical; higher $CaCl_2$ (10–20%) accelerated fusion and partial disintegration, yielding turbid baths (Fig. 2). These outcomes are characteristic of ionotropic systems at low polymer content causes weak networks and/or excess crosslinker lead to rapid surface-hardening, widely reported for Ca^{2+}-gelled polysaccharide beads.[20,21]

Raising starch to 10% markedly improved morphology. F2.1 (5% $CaCl_2$) gave discrete, opaque-white, spherical beads and was the most robust condition; F2.2 (10% $CaCl_2$) also formed good beads but with modest turbidity, indicating minor leaching; F2.3–F2.4 (15–20% $CaCl_2$) increasingly showed fusion/cloudiness (Fig. 2). The window of moderate $CaCl_2$ (5–10%) with intermediate polymer (≈10%) aligns with optimized ionotropic gelation where gelation is fast enough to set the droplet but not so fast as to cause shell-hardening and aggregation.[20,21] Comparable starch beads prepared by emulsion/gelation and freeze-drying also show

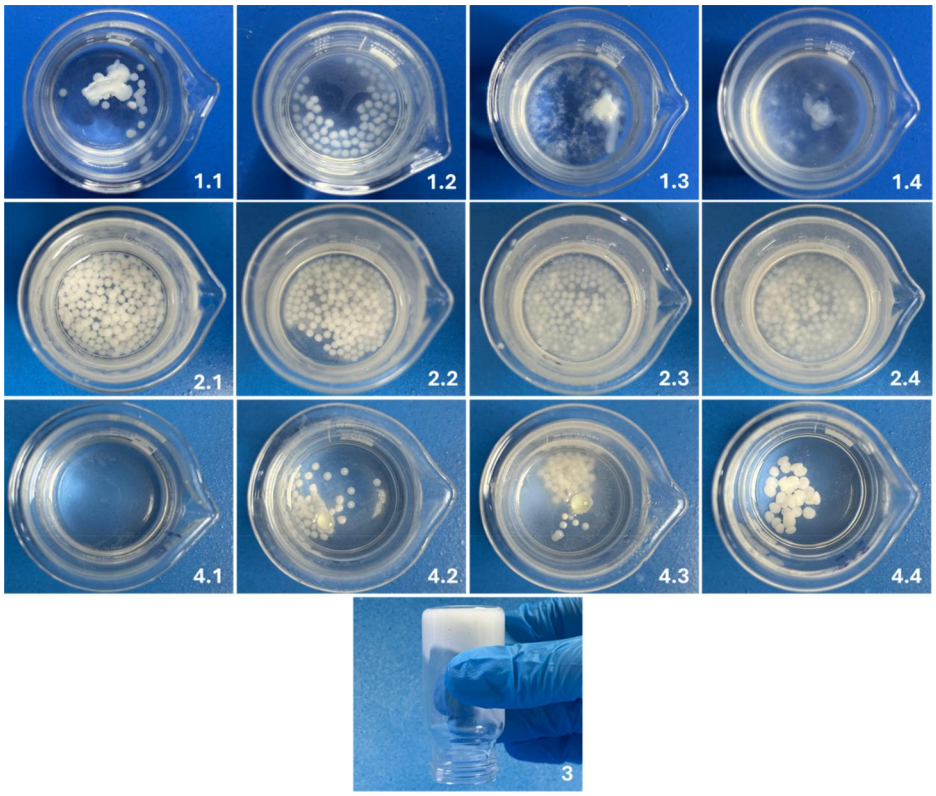

Figure 2. Macroscopic appearance of starch beads synthesized under different preformulation conditions. F1 showed aggregation and incomplete bead formation, whereas F2 produced more uniform and stable spherical structures. Higher starch concentration (F3) led to bulk gelation, while F4 displayed irregular morphologies depending on NaOH content.

stable beads and high structural integrity under similar solids levels.[22]

The paste was too viscous to handle reproducibly in F3 (Fig. 2). Hot dropping partially mitigated premature gelation but yielded deformed, droplet-like particles; the series was discontinued. This reflects the processing limits at high starch solids in high-amylose gels, where viscosity and rapid structuring hinder the reliable droplet formation.[23]

With 0.1% NaOH (F4.1), droplets dispersed immediately (no bead formed), indicating insufficient gelatinization. At 0.5% (F4.2), irregular/fragmented shapes formed. About 2% (F4.3) produced partial beads but entrapped air and later coalesced; 3% (F4.4) showed incomplete starch dissolution and unstable beads with turbidity (Fig. 2). These trends match the alkali window reported for high-amylose corn starch: mild NaOH (≈1–2%) effectively swells/solubilizes amylose and lowers order, whereas too little alkali fails to gelatinize and too much promotes structural degradation/heterogeneity.[17,24]

Combining our observations with the literature, the most reproducible, morphologically stable, and workable conditions were F2.1, F2.2, and F2.3. Lower starch (5%) lacks network strength; very high starch (15%) is impractically viscous; very low NaOH prevents gelatinization; very high NaOH yields heterogeneous pastes; and excessive $CaCl_2$ drives shell-hardening and fusion. These conclusions are consistent with alkali-assisted gelatinization/de-ordering in high-amylose starch,[17] physical Ca^{2+} coordination with starch hydroxyls,[18] and ionotropic gelation windows described for Ca^{2+}-gelled polysaccharides.[21]

3.2. Morphological analysis (SEM)

Representative SEM micrographs of the lyophilized beads prepared from F2.2 formulation are shown in Fig. 3. At low magnification, the beads retained an overall spherical morphology with intact geometry (Fig. 4a). The external surfaces appeared rough, exhibiting irregularities and shallow depressions, as well as surface pores of variable sizes (Fig. 3(B)). Such features are characteristic of ionically crosslinked starch-based hydrogels after freeze-drying, where sublimation of ice crystals during lyophilization leaves behind a porous matrix.[25]

Cross-sectional SEM images revealed an interconnected sponge-like porous network (Fig. 4c). At higher magnification (100×), this network appeared as densely distributed micropores (Fig. 3(D)). Quantitative pore-size analysis indicated a median equivalent pore diameter of ∼18.7 µm (mean ± SD: 20.7 ± 8.4 µm, $n = 577$; IQR: 13.2–25.4 µm), which is within the range reported for Ca^{2+}-crosslinked starch cryogels and aerogels, where typical pore sizes span from 10 to 50 µm depending on crosslinking and processing conditions.[18,26] The porous network observed here is consistent with previous reports showing that ionic crosslinking with calcium generates finer and more homogeneous pore structures compared to non-crosslinked starch gels.[18]

Overall, SEM analysis confirmed that the Ca^{2+}-crosslinked high-amylose starch beads maintained their spherical integrity after lyophilization while developing a well-connected microporous structure.

From a functional standpoint, the preserved spherical morphology supports ease of handling and potential catheter/trocar-assisted placement, whereas the microporous interior provides aqueous pathways expected to facilitate imbibition and mitigate burst while enabling sustained release.[27] In the context of enzyme-rich environments (e.g., pancreatic milieu), such a network is also compatible with controlled erosion, as pore interconnectivity can mediate enzyme ingress while cross-link density tempers degradation-features aligned with the depot concept explored in this study.[28] Collectively, the SEM results corroborate that the Ca^{2+}-crosslinked starch beads combine the geometric integrity with a transport-competent microporosity conducive to localized drug delivery.

3.3. Swelling tests

All formulations demonstrated an initial rapid mass decline during the first 6–9 h, followed by a slower decay and approach to equilibrium (Fig. 4). This biphasic swelling profile reflects early-stage ion exchange and loosening of loosely bound water and Ca^{2+}, followed by stabilization of the polymer network—a behavior commonly noted in ionically crosslinked polysaccharide hydrogels.[5,29]

F2.1 lost integrity for measurement beyond ~48 h under all pH conditions, indicating insufficient crosslinking due to lower $CaCl_2$ content. Similar outcomes were reported in low-crosslinked alginate systems where beads disintegrated rapidly.[20] F2.2 and F2.3 maintained integrity throughout the study, highlighting that higher Ca^{2+} levels enhanced network robustness, consistent with other observations in polysaccharide hydrogels.[18,30]

At the pH 3, beads showed the lowest mass loss, likely due to suppressed hydroxyl deprotonation and stronger hydrogen-bonding that restrict network swelling, consistent with behavior observed in other starch-based hydrogels.[5,31] At the pH 7.4, greater mass loss occurred, likely due to phosphate ions displacing Ca^{2+} in the network and weakening ionic crosslinks—a phenomenon seen in calcium-crosslinked polysaccharide matrices.[20,32] At the pH 8, maximum erosion observed, as expected from increased hydroxyl ionization that disrupts hydrogen bonding and leads to network loosening—consistent with swelling trends in starch matrices under the alkaline conditions.[33]

The data confirm that both Ca^{2+} concentration and environmental pH critically determine bead stability. F2.2 and F2.3 showed superior swelling resistance across environmental conditions, while F2.1's insufficient crosslinking led to early disintegration. These findings align with the broader polysaccharide hydrogel studies highlighting the importance of optimized crosslinking for network integrity in different pH environments.[18,20]

Together, the swelling and degradation results highlight the intrinsic hydrogel behavior of the Ca^{2+}-crosslinked starch matrix. The network acts as a hydrated, ionically stabilized gel, where crosslink density and porosity jointly determine water uptake, mechanical stability, and enzymatic accessibility. These correlations clarify the structural basis of the observed hydrogel characteristics and their relevance to controlled drug release.

From a biomedical perspective, the retention of spherical integrity for F2.2 and F2.3 under near-physiological conditions suggests residence times of several days—clinically relevant for intratumoral depots. In the context of localized chemotherapy, depot formulations that maintain structural integrity can ensure prolonged local drug exposure while minimizing systemic diffusion or washout (e.g., *in situ* depot hydrogels have been engineered to provide multi-day retention in tumor tissue).[34] The balance between gradual erosion and structural persistence is particularly valuable for drug delivery, as controlled disintegration can temper burst release while permitting sustained drug transport. Similar

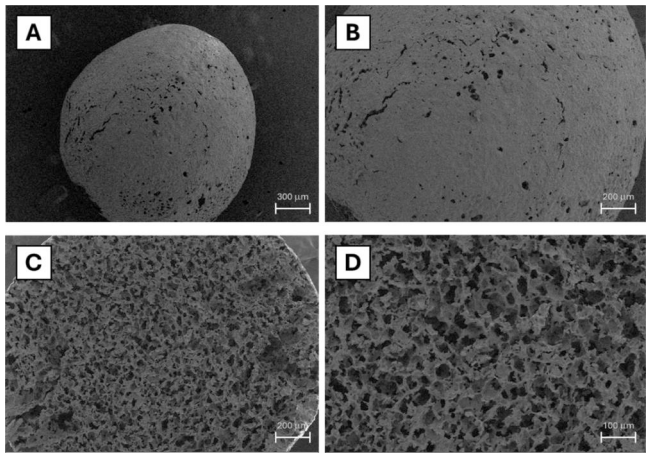

Figure 3. SEM images of lyophilized starch beads prepared from F2.2 formulation. (A) Overall spherical morphology, (B) surface view showing pores and roughness, (C) cross-sectional view demonstrating the porous inner network, and (D) high-magnification image highlighting the microporous structure.

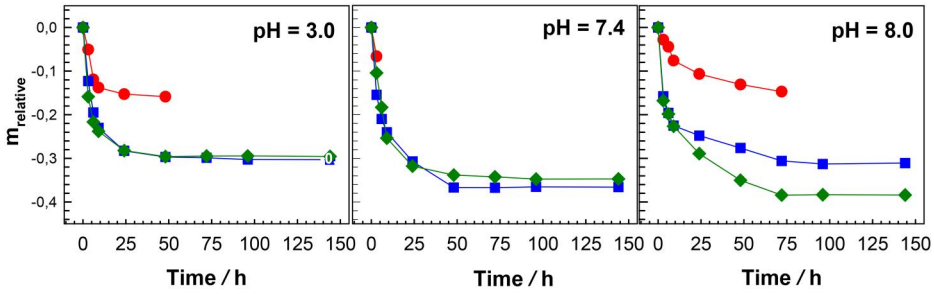

Figure 4. Relative mass change of starch-Ca^{2+} beads prepared from F2.1 (circle), F2.2 (square), and F2.3 (diamond) in three buffer environments: acidic buffer (pH 3), PBS (pH 7.4), and alkaline buffer (pH 8). Measurements were performed up to 144 h with buffer renewal at each time point. Data illustrate the effect of $CaCl_2$ concentration and environmental pH on bead swelling and structural stability.

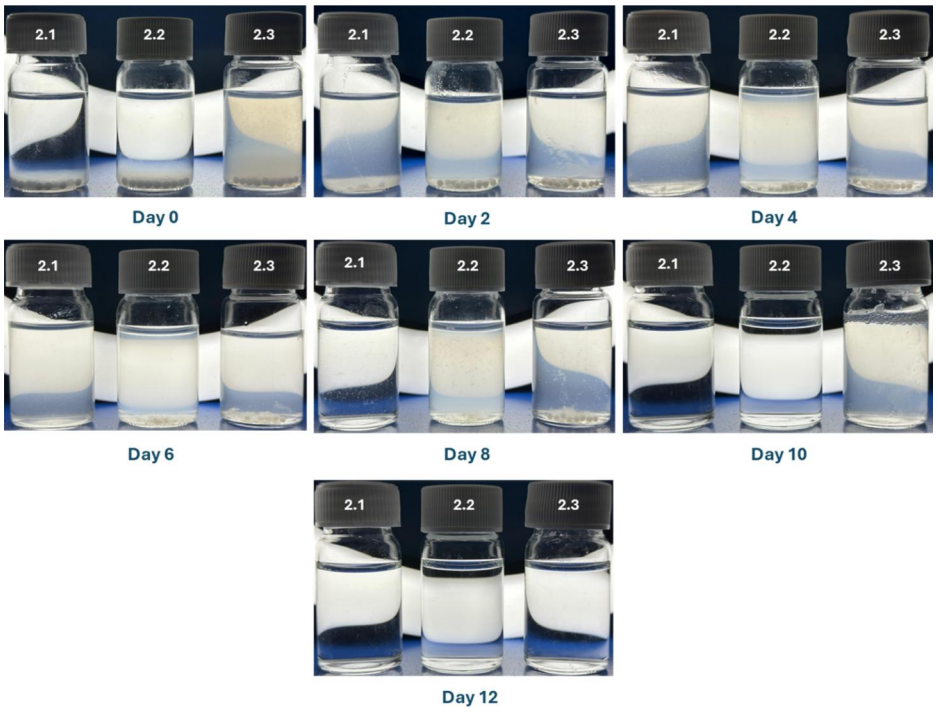

Figure 5. Visual monitoring of enzymatic degradation of starch-Ca^{2+} beads (F2.1, F2.2, and F2.3) in PBS containing α-amylase (1 mg/mL) at 37 °C. Images were recorded at predetermined time intervals up to 12 days.

design principles have been described in reviews of cross-linked gels for drug delivery, where the integrity of the network and controlled degradation kinetics are key to mitigating initial burst and achieving sustained release profiles.[35,36] Thus, the swelling data support that optimized Ca^{2+} cross-linking (10–15% $CaCl_2$) produces starch beads with favorable stability profiles for localized chemotherapy.

3.4. a-amylase sensitivity tests

Time-lapse images revealed gradual erosion and disintegration of the beads in the presence of 1 mg/mL α-amylase in PBS (pH 7.4): F2.1 completely disintegrated on day 6, F2.2 on day 8, and F2.3 on day 10 (Fig. 5). This order of stability (F2.3 > F2.2 > F2.1) suggests that increasing the $CaCl_2$ concentration (15%, 10%, 5%, respectively) increases the density of ionic bridges/nodes in the gel network, thus limiting enzyme diffusion and the accessibility of glycosidic bonds. The ability of gelatinized starch to network with Ca^{2+} and increase network stiffness has been reported in starch-based systems; tighter networks are more resistant to enzymatic degradation. This trend is consistent with the classical studies showing that the rate of degradation by α-amylase decreases as the crosslink density increases in crosslinked starch microspheres.[37]

Mechanistically, α-amylase first targets amorphous regions; as hydrolysis progresses, relatively more ordered/crystalline regions increase, and enzyme sensitivity decreases.[38] The increased turbidity observed in the experiment are consistent with what has been described in the literature as surface-controlled erosion of cross-linked starch microspheres.[39]

From a translational standpoint, the differential degradation profiles observed here are highly relevant to the pancreatic tumor microenvironment, which is physiologically rich in digestive enzyme secretion (e.g., acinar cells produce amylase, proteases) and local enzymatic activity within tumor stroma (e.g., ECM-degrading enzymes).[40] The enzyme-triggered erosion behavior further supports the hydrogel-like nature of the network, in which enzymatic attack initiates from amorphous domains and gradually propagates through the crosslinked matrix. This behavior is characteristic of degradable hydrogels and indicates a balance between network integrity and controlled disintegration. The persistence of F2.2 and F2.3 beads for 8–10 days suggests a clinically relevant residence time, sufficient to permit sustained intratumoral release of gemcitabine while avoiding long-term persistence of foreign material. Controlled enzymatic erosion is particularly advantageous, as it provides a built-in clearance mechanism following local therapy—a design strategy widely discussed in reviews of enzyme-responsive hydrogels and biomaterials for localized drug delivery systems.[41]

3.5. Mechanical tests

The uniaxial compression tests revealed significant differences in stiffness among the starch-Ca^{2+} bead formulations (Fig. 6). F2.1 exhibited the lowest Young's modulus (~12 kPa), F2.2 showed an intermediate value (~15 kPa), and F2.3 demonstrated a markedly higher modulus (~35 kPa). These results indicate that increasing starch and Ca^{2+} concentrations significantly enhance the mechanical rigidity and load-bearing capability of the hydrogel network.

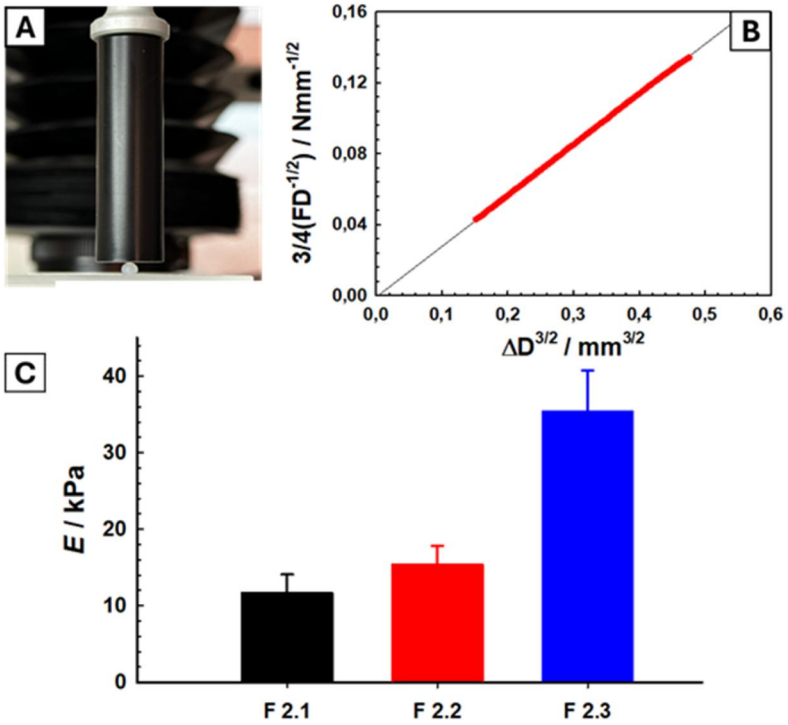

Figure 6. Single-bead compression to estimate stiffness. (A) Parallel-plate setup with a bead. (B) Hertzian analysis: linear plot of $(3/4)\,F\,D^{-1/2}$ vs. $\Delta D^{3/2}$; the slope yields the apparent Young's modulus E. (C) E (kPa, mean ± SD) for F2.1–F2.3, showing increasing stiffness with higher $CaCl_2$ content. Data are presented as mean ± SD ($n = 10$).

These values align well with the reported range for ionically crosslinked polysaccharide hydrogels, which typically exhibit Young's moduli from tens of kPa up to several hundred kPa, depending on polymer composition and crosslink density.[42] Specifically, alginate hydrogels crosslinked with Ca^{2+} exhibit moduli between ~5–20 kPa, depending on $CaCl_2$ concentration and gel properties.[43] Although starch-based systems may differ structurally, the mechanical trend is consistent: higher crosslinking yields higher stiffness.

Notably, the magnitude of F2.3′s modulus (~35 kPa) suggests a robust hydrogel structure capable of withstanding mechanical stresses—unlike more deformable gels (e.g., F2.1) that may facilitate rapid swelling and drug release but compromise structural integrity during handling or physiological transit. This stiffness gradient across formulations offers a tunable mechanical profile: softer beads (e.g., F2.1) may facilitate short-term release but are mechanically fragile, whereas increasing cross-link density typically yields stiffer networks that better tolerate handling and compressive loads during implantation, a trend widely reported for ionically cross-linked polysaccharide hydrogels and alginate beads.[44] Stiffer beads (F2.3) therefore withstand handling and offer prolonged stability, consistent with observations that higher Ca^{2+} levels and optimized formulations increase modulus and extend dissolution/erosion times in calcium-gelled carriers.[42] The intermediate formulation (F2.2) provides a balance between stability and flexibility, aligning with the concept of tissue-matched mechanics for local delivery depots—hydrogels designed with moduli in the soft-tissue range minimize iatrogenic damage and integrate more favorably with host tissue.[45] The mechanical properties further corroborate the hydrogel character of the system, as the measured moduli (10–35 kPa) fall within the range typical for soft polysaccharide-based hydrogels, confirming that the Ca^{2+}-crosslinked starch beads form a stable yet deformable gel network. In sum, selecting intermediate stiffness while retaining biodegradability supports gradual resorption and sustained local exposure—key goals highlighted across translational hydrogel depot literature.[34,46]

3.6. Quantification of gemcitabine by HPLC

Calibration of gemcitabine over 10–60 µg mL^{-1} produced an excellent linear response ($y = 380,89x - 991,26$); $R^2 = 0.9999$; Figure S5). This working range, C18 phase, MeOH/phosphate buffer (40:60, v/v), and UV 270 nm detection are in close agreement with prior stability—indicating RP-HPLC methods for gemcitabine, which likewise reported linearity across 10–60 µg mL^{-1} and short retention times around ~2.3 min under comparable conditions. Retention time remained stable in our assay at ~2.85 min, consistent with the range reported for similar mobile phases and column geometry.[47]

Precision was assessed across two consecutive days at 30, 40, and 50 µg mL^{-1}, yielding %RSD $\leq$ 0.3% at all levels, which demonstrates excellent day-to-day repeatability (Table S1). In line with ICH Q2(R1), this corresponds to intermediate precision (within-laboratory, between-day variability) and, together with repeatability, evidences method robustness for quantitative use; ICH defines these precision tiers and recommends reporting variability as %RSD but does not impose a universal numeric threshold.[48]

Overall, the strong linearity, stable retention, and low interday variability support this HPLC-UV method as a reliable platform for quantifying gemcitabine in our Ca^{2+}–

starch bead workflow (EE% and release). Comparable HPLC-UV assays have been successfully applied to gemcitabine in pharmaceutical and biological matrices, reinforcing the suitability of our approach.[49]

3.7. Drug loading and encapsulation efficiency

FTIR analysis was performed (Figure S4) to confirm the presence and effect of GEM within the starch beads prior to evaluating their drug loading capacities. In the gemcitabine spectrum, NH_2/NH_2 stretches (including the band at ≈ 3,390 cm^{-1}) and the $C=O/NH_2$ bending region in the pyrimidine ring (≈ 1,690–1,630 cm^{-1}) are prominent; C-F stretches also typically appear in the range ≈ 1,000–1,400 cm^{-1}. In the composite (GEM-Hylon VII-Ca^{2+}), these features overlap, broaden, and slightly displace the starch fingerprint bands; however, no new characteristic bands indicating new covalent bonds appear. This suggests that loading occurs *via* physical retention/hydrogen bonding and that GEM is not chemically modified. A similar approach is used in studies where loading of GEM onto polymeric carriers is confirmed by FTIR.[50]

In the drug-loaded sample, additional absorption/intensity increases were observed around ≈ 1,650 cm^{-1} (ring $C=O/NH_2$ band of GEM) and around ≈ 1,080–1,050 cm^{-1} (C-F/C-O contribution), supporting the presence of GEM in the matrix. At the same time, small changes (broadening/position shift) in the O-H band indicate hydrogen bonding between the starch hydroxyls and the -OH/NH_2 groups of GEM. Such band shifts are consistent with the expected weak interaction pattern in polymer-drug systems.[51] FTIR results show cross-linking consistent with the strengthened interactions around the -OH in the starch network in the presence of Ca^{2+}, GEM was loaded into the matrix while maintaining its chemical structure, and no new covalent bond formation, which is consistent with the depot concept for local release in the study.[52]

Encapsulation efficiency was calculated from the mass balance between the initial drug in the feed and the non-entrapped fraction quantified in the $CaCl_2$ curing supernatant. Using a feed of 0.50 mL at 5 mg mL^{-1} gemcitabine and a measured supernatant content of 2396,66 ± 1,68 µg, the entrapped amount was 103,34 ± 1,68 µg for 30 beads, corresponding to EE = 4.14%±0.7 (3.44 ± 0,06 µg $bead^{-1}$). The low EE is mechanistically consistent with gemcitabine's pronounced hydrophilicity (negative logP and high aqueous solubility), which disfavors retention in hydrophilic gel networks and promotes partitioning to the external aqueous phase during gelation.[53,54]

In ionotropic gelation processes, EE is highly sensitive to formulation and process parameters (polymer and Ca^{2+} levels, hardening/curing time, and external phase conditions). Prolonged residence in the crosslinking bath and strong sink conditions facilitate diffusive loss (leaching) of hydrophilic actives from forming beads, leading to lower entrapment—an effect broadly documented across Ca^{2+}-gelled polysaccharide systems and reviews on alginate/gellan platforms.[55,56] In comparable calcium-alginate bead systems, encapsulation efficiency is likewise governed by these variables, with the optimized conditions yielding markedly higher entrapment than non-optimized curing protocols.[57]

3.8. In vitro release

Gemcitabine release from Ca^{2+}-starch beads displayed a burst-to-plateau profile: cumulative release reached ∼70% at 0.1 h, ∼90% by ∼0.5 h, ∼95% by ∼1 h, and approached ∼99% by ∼5 h, remaining at a plateau through 24–48 h. The absolute mass released tracked the same trend and approached the loaded dose (∼99%), supporting mass balance and the validity of the sampling-with-replacement calculation (Fig. 7). Correcting cumulative amounts for aliquot removal and volume replacement is recommended in dissolution/release assays to avoid profile distortion, especially at early time points.[58]

The rapid early release is consistent with the high aqueous solubility and hydrophilicity of gemcitabine, which favors partitioning into the external medium, particularly when sink conditions are used.[59] In dissolution methodology, sink promotes a strong concentration gradient and accelerates release—conditions that can emphasize burst from hydrophilic matrices.[60] Similar burst-dominated behavior is widely reported for ionotropically gelled polysaccharide carriers, where process variables (polymer level, crosslinking, bath volume/time) govern early loss and overall kinetics.[55] Comprehensive hydrogel reviews likewise note

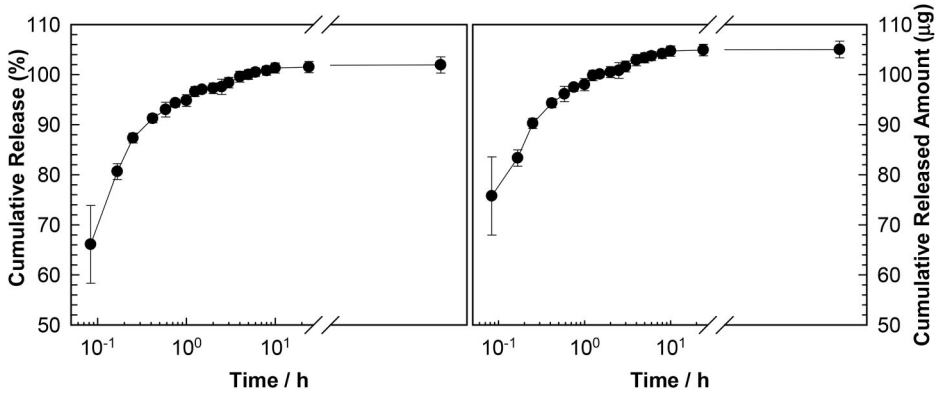

Figure 7. *In vitro* release of gemcitabine from Ca^{2+}-crosslinked high-amylose starch beads in PBS (pH 6.6, 37 °C). Left: cumulative release (%). Right: cumulative amount (µg). Data = mean ± SD; sample-replacement correction applied $m_i = VC_i + v \cdot \sum_{j=1}^{i-1} C_j$

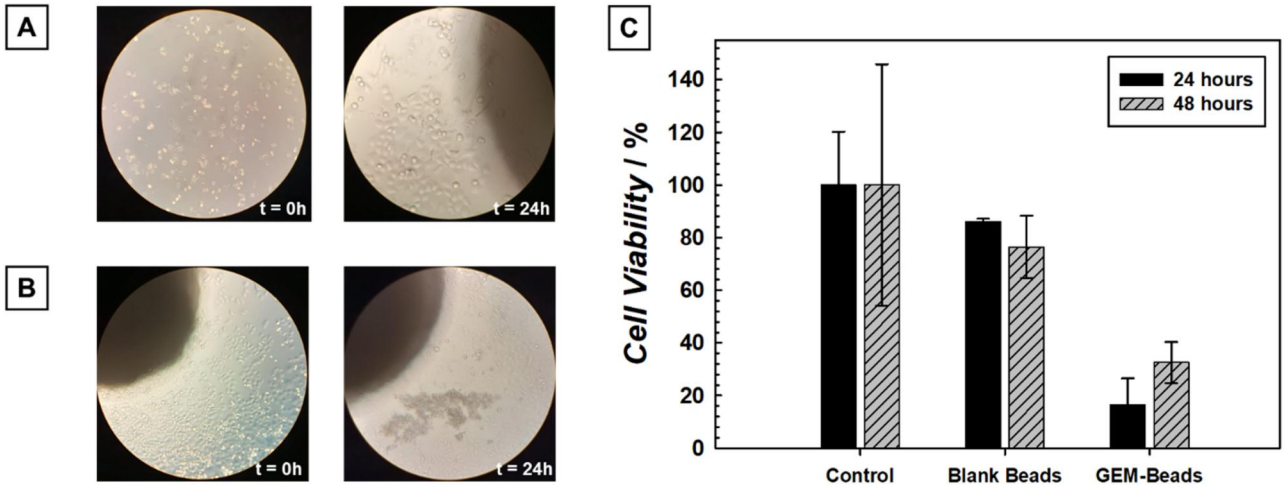

Figure 8. *In vitro* evaluation of starch beads on PANC-1 cells. (A-B) Microscopy images showing cells treated with blank and GEM-loaded beads at $t = 0$ h and $t = 24$ h. (C) MTT assay results showing cell viability of control, blank beads, and gemcitabine-loaded beads at 24 h and 48 h. Data represent mean ± SD ($n = 3$).

that small, water-soluble actives often show fast initial diffusion from hydrophilic, microporous networks under sink, unless additional barriers (coatings/multilayers or denser crosslinking) are introduced.[61]

Collectively, these results indicate that in the present formulation diffusion of surface/near-surface drug under sink conditions dominates the early phase, yielding a rapid approach to completion. Reducing burst in future iterations may require network densification or secondary coatings and/or less aggressive sink during curing/loading to limit near-surface drug accumulation, as suggested in the ionotropic-gelation literature.[55]

3.9. In vitro efficacy tests

Microscopic examination at 24 h shows that the blank starch beads exposure produce no observable change in cell morphology or density compared to the untreated control. In contrast, cells exposed to gemcitabine-loaded beads exposition display a marked reduction in confluency, rounding, and detachment (Fig. 8(A-B)).

Quantitatively, *via* MTT assay, both the control group and the blank beads group maintain high cell viability (∼100%) at both 24 h and 48 h. In the gemcitabine-loaded beads group, cell viability drops sharply—approximately 15% at 24 h, and increases modestly to around 30% at 48 h (mean ± SD, $n = 3$). These results indicate that the empty beads are essentially nontoxic under experimental conditions, whereas the loaded beads deliver cytotoxic effects consistent with the presence of gemcitabine.

The fact that cell viability at 48 h with the loaded beads remains lower than with blank beads suggests sustained or prolonged exposure, better protection of gemcitabine from deactivation, or enhanced cellular uptake afforded by the bead matrix. These mechanisms have been proposed in the literature (e.g. nanoparticulate gemcitabine formulations) to explain efficacy.[62]

Overall, the results support that starch/Ca^{2+} beads are *in vitro* tolerable when blank, whereas gemcitabine loading imparts substantial cytotoxicity in PANC-1 cells. This suggests that the carrier system is promising for local delivery of gemcitabine.

4. Conclusion

Here we present, to our knowledge, the first spherical high-amylose starch beads produced by droplet-gelation and Ca^{2+} ionotropic crosslinking as a simple, water-based depot for locoregional PDAC chemotherapy. The beads preserve spherical geometry with microporous interiors (SEM); FTIR supports Ca^{2+}-OH interactions in the starch network and non-covalent gemcitabine loading. Optimized $CaCl_2$ (10–15%) yields beads that remain intact in PBS yet undergo enzyme-responsive erosion (α-amylase, ∼8–10 days). HPLC-UV showed the modest loading (EE ≈ 4.24%, ∼3.53 µg/bead) and burst-to-plateau release under sink with near-quantitative mass recovery, while drug-loaded beads displayed *in vitro* cytotoxicity in PANC-1 cells. Overall, Ca^{2+}-starch depots are in-vitro tolerable, solvent-free, and injection-ready, supporting their potential for intratumoral delivery; future work will focus on boosting EE, tempering burst (coatings/densification, process optimization), and *in vivo* validation of residence, pharmacokinetics, and safety.

Disclosure Statement

The authors declare no competing financial interest.

Funding

This study was financially supported by the Scientific Research Projects Committee of Bezmialem Vakif University (BAP, 20240911), Istanbul, Turkey.

References

[1] Olajubutu, O.; Ogundipe, O. D.; Adebayo, A.; Adesina, S. K. Drug Delivery Strategies for the Treatment of Pancreatic Cancer. *Pharmaceutics* **2023**, *15*, 1318. DOI: 10.3390/pharmaceutics15051318.

[2] Thompson, B. R.; Shi, J.; Zhu, H.-J.; Smith, D. E. Pharmacokinetics of Gemcitabine and Its Amino Acid Ester Prodrug following Intravenous and Oral Administrations in Mice. *Biochem. Pharmacol.* **2020**, *180*, 114127. DOI: 10.1016/j.bcp.2020.114127.

[3] Hosein, A. N.; Brekken, R. A.; Maitra, A. Pancreatic Cancer Stroma: An Update on Therapeutic Targeting Strategies. *Nat. Rev. Gastroenterol. Hepatol.* **2020**, *17*, 487–505. DOI: 10.1038/s41575-020-0300-1.

[4] Levy, M. J.; Alberts, S. R.; Bamlet, W. R.; Burch, P. A.; Farnell, M. B.; Gleeson, F. C.; Haddock, M. G.; Kendrick, M. L.; Oberg, A. L.; Petersen, G. M.; et al. EUS-Guided Fine-Needle Injection of Gemcitabine for Locally Advanced and Metastatic Pancreatic Cancer. *Gastrointest. Endosc.* **2017**, *86*, 161–169. DOI: 10.1016/j.gie.2016.11.014.

[5] Lee, C. S.; Hwang, H. S. Starch-Based Hydrogels as a Drug Delivery System in Biomedical Applications. *Gels* **2023**, *9*, 951. DOI: 10.3390/gels9120951.

[6] Date, K.; Satoh, A.; Iida, K.; Ogawa, H. Pancreatic α-Amylase Controls Glucose Assimilation by Duodenal Retrieval through N-Glycan-Specific Binding, Endocytosis, and Degradation. *J. Biol. Chem.* **2015**, *290*, 17439–17450. DOI: 10.1074/jbc.M114.594937.

[7] Wang, Y.; Shen, Z.; Wang, H.; Song, Z.; Yu, D.; Li, G.; Liu, X.; Liu, W. Progress in Research on Metal Ion Crosslinking Alginate-Based Gels. *Gels* **2024**, *11*, 16. DOI: 10.3390/gels11010016.

[8] Besiri, IN.; Goudoulas, T. B.; Fattahi, E.; Becker, T. Experimental Advances in the Real-Time Recording of Cross-Linking Alginate In Situ Gelation: A Review. *Polymers (Basel)* **2023**, *15*, 2875. DOI: 10.3390/polym15132875.

[9] Hamdi, G.; Ponchel, G.; Duchêne, D. Formulation of Epichlorohydrin Cross-Linked Starch Microspheres. *J. Microencapsul.* **2001**, *18*, 373–383. DOI: 10.1080/02652040010019505.

[10] Kumar, Y.; Singh, S.; Saxena, D. C. Effect of Citric Acid and Sodium Trimetaphosphate Induced Crosslinking on Functional, Rheological, Structural, and Thermal Properties of Buckwheat Starch. *Starch-Stärke* **2023**, *75*, 2200267.

[11] Xu, K.; Tan, L.; Sun, H.; Chong, C.; Li, L.; Sun, B.; Yao, Z.; Zhuang, Y.; Wang, L. Manipulating Gelatinization, Retrogradation, and Hydrogel Properties of Potato Starch through Calcium Chloride-Controlled Crosslinking and Crystallization Behavior. *Carbohydr. Polym.* **2025**, *357*, 123371. DOI: 10.1016/j.carbpol.2025.123371.

[12] Hertz, H. Ueber die Berührung fester elastischer Körper. 1882.

[13] Barquins, M.; Shanahan, M. E. Effect of Surface Cavities on Static and Dynamic Adhesion to an Elastomer. *Int. J. Adhes. Adhes.* **1997**, *17*, 313–317. DOI: 10.1016/S0143-7496(97)00017-1.

[14] Lu, W.-M.; Tung, K.-L.; Hung, S.-M.; Shiau, J.-S.; Hwang, K.-J. Compression of Deformable Gel Particles. *Powder Technol.* **2001**, *116*, 1–12. DOI: 10.1016/S0032-5910(00)00357-0.

[15] Mastanamma, S.; Ramkumar, G.; Kumar, D. A.; Rao, J. V. L. N. S. A Stability Indicating RP-HPLC Method for the Estimation of Gemcitabine HCl in Injectable Dosage Forms. *J. Chem.* **2010**, *7*, 239–244. DOI: 10.1155/2010/724915.

[16] Gao, F.; Zhang, Y.; Li, Y.; Xu, B.; Cao, Z.; Liu, W. Sea Cucumber-Inspired Autolytic Hydrogels Exhibiting Tunable High Mechanical Performances, Repairability, and Reusability. *ACS Appl. Mater Interfaces* **2016**, *8*, 8956–8966. DOI: 10.1021/acsami.6b00912.

[17] Qin, Y.; Zhang, H.; Dai, Y.; Hou, H.; Dong, H. Effect of Alkali Treatment on Structure and Properties of High Amylose Corn Starch Film. *Materials (Basel)* **2019**, *12*, DOI: 10.3390/ma12101705.

[18] Boonkanon, C.; Phatthanawiwat, K.; Chuenchom, L.; Lamthornkit, N.; Taweekarn, T.; Wongniramaikul, W.; Choodum, A. Preparation and Characterization of Calcium Cross-Linked Starch Monolithic Cryogels and Their Application as Cost-Effective Green Filters. *Polymers (Basel)* **2021**, *13*, 3975. DOI: 10.3390/polym13223975.

[19] Monograph, N. Infrared spectroscopy of carbohydrates A review of the literature. 1968.

[20] Tavakol, M.; Vasheghani-Farahani, E.; Hashemi-Najafabadi, S. The Effect of Polymer and CaCl(2) Concentrations on the Sulfasalazine Release from alginate-N,O-Carboxymethyl Chitosan Beads. *Prog. Biomater.* **2013**, *2*, 10. DOI: 10.1186/2194-0517-2-10.

[21] Bennacef, C.; Desobry, S.; Jasniewski, J.; Leclerc, S.; Probst, L.; Desobry-Banon, S. Influence of Alginate Properties and Calcium Chloride Concentration on Alginate Bead Reticulation and Size: A Phenomenological Approach. *Polymers (Basel)* **2023**, *15*, 4163. DOI: 10.3390/polym15204163.

[22] Wang, M.; Ji, N.; Li, M.; Li, Y.; Dai, L.; Zhou, L.; Xiong, L.; Sun, Q. Fabrication and Characterization of Starch Beads Formed by a Dispersion-Inverse Gelation Process for Loading Polyphenols with Improved Antioxidation. *Food Hydrocolloids* **2020**, *101*, 105565. DOI: 10.1016/j.foodhyd.2019.105565.

[23] Cheng, Y.; Yuqing, H.; Xiao, L.; Gao, W.; Kang, X.; Sui, J.; Cui, B. Impact of Starch Amylose and Amylopectin on the Rheological and 3D Printing Properties of Corn Starch. *Int. J. Biol. Macromol.* **2024**, *278*, 134403. DOI: 10.1016/j.ijbiomac.2024.134403.

[24] Wang, S.; Copeland, L. Effect of Alkali Treatment on Structure and Function of Pea Starch Granules. *Food Chem.* **2012**, *135*, 1635–1642. DOI: 10.1016/j.foodchem.2012.06.003.

[25] Ahmadzadeh, S.; Ubeyitogullari, A. Fabrication of Porous Spherical Beads from Corn Starch by Using a 3D Food Printing System. *Foods* **2022**, *11*, 913. DOI: 10.3390/foods11070913.

[26] Abhari, N.; Madadlou, A.; Dini, A. Structure of Starch Aerogel as Affected by Crosslinking and Feasibility Assessment of the Aerogel for an anti-Fungal Volatile Release. *Food Chem.* **2017**, *221*, 147–152. DOI: 10.1016/j.foodchem.2016.10.072.

[27] Hernandez, J. L.; Woodrow, K. A. Medical Applications of Porous Biomaterials: Features of Porosity and Tissue-Specific Implications for Biocompatibility. *Adv. Healthc. Mater.* **2022**, *11*, e2102087. DOI: 10.1002/adhm.202102087.

[28] Feng, S.; Chen, K.; Wang, S. Practical Guide to the Design of Granular Hydrogels for Customizing Complex Cellular Microenvironments. *Adv. Healthc. Mater.* **2025**, *14*, e01947. DOI: 10.1002/adhm.202501947.

[29] Bajpai, S. K.; Sharma, S. Investigation of Swelling/Degradation Behaviour of Alginate Beads Crosslinked with Ca2+ and Ba2+ Ions. *React. Funct. Polym.* **2004**, *59*, 129–140. DOI: 10.1016/j.reactfunctpolym.2004.01.002.

[30] da Silva Fernandes, R.; Tanaka, F. N.; de Moura, M. R.; Aouada, F. A. Development of Alginate/Starch-Based Hydrogels Crosslinked with Different Ions: Hydrophilic, Kinetic and Spectroscopic Properties. *Mater. Today Commun.* **2019**, *21*, 100636. DOI: 10.1016/j.mtcomm.2019.100636.

[31] Koshenaj, K.; Ferrari, G. A Comprehensive Review on Starch-Based Hydrogels: From Tradition to Innovation, Opportunities, and Drawbacks. *Polymers (Basel)* **2024**, *16*, 1991. DOI: 10.3390/polym16141991.

[32] Jing, H.; Huang, X.; Du, X.; Mo, L.; Ma, C.; Wang, H. Facile Synthesis of pH-Responsive Sodium Alginate/Carboxymethyl Chitosan Hydrogel Beads Promoted by Hydrogen Bond. *Carbohydr. Polym.* **2022**, *278*, 118993. DOI: 10.1016/j.carbpol.2021.118993.

[33] Shivakumara, L. R.; Demappa, T. Synthesis and Swelling Behavior of Sodium Alginate/Poly(Vinyl Alcohol) Hydrogels. *Turk. J. Pharm. Sci.* **2019**, *16*, 252–260. DOI: 10.4274/tjps.galenos.2018.92408.

[34] Shin, G. R.; Kim, H. E.; Kim, J. H.; Choi, S.; Kim, M. S. Advances in Injectable In Situ-Forming Hydrogels for Intratumoral Treatment. *Pharmaceutics* **2021**, *13*, 1953. DOI: 10.3390/pharmaceutics13111953.

[35] Mikhail, A. S.; Morhard, R.; Mauda-Havakuk, M.; Kassin, M.; Arrichiello, A.; Wood, B. J. Hydrogel Drug Delivery Systems

for Minimally Invasive Local Immunotherapy of Cancer. *Adv. Drug Deliv. Rev.* **2023**, *202*, 115083. DOI: 10.1016/j.addr.2023.115083.

[36] Mashabela, L. T.; Maboa, M. M.; Miya, N. F.; Ajayi, T. O.; Chasara, R. S.; Milne, M.; Mokhele, S.; Demana, P. H.; Witika, B. A.; Siwe-Noundou, X.; et al. A Comprehensive Review of Cross-Linked Gels as Vehicles for Drug Delivery to Treat Central Nervous System Disorders. *Gels* **2022**, *8*, 563. DOI: 10.3390/gels8090563.

[37] Xiao, H.; Lin, Q.; Liu, G. Q. Effect of Cross-Linking and Enzymatic Hydrolysis Composite Modification on the Properties of Rice Starches. *Molecules* **2012**, *17*, 8136–8146. DOI: 10.3390/molecules17078136.

[38] Zhang, M.; Jia, H.; Wang, B.; Ma, C.; He, F.; Fan, Q.; Liu, W. A Prospective Review on the Research Progress of Citric Acid Modified Starch. *Foods* **2023**, *12*. DOI: 10.3390/foods12030458.

[39] Hamdi, G.; Ponchel, G. Enzymatic Degradation of Epichlorohydrin Crosslinked Starch Microspheres by α-Amylase. *Pharm Res.* **1999**, *16*, 867–875. DOI: 10.1023/a:1018878120100.

[40] Hartupee, C.; Nagalo, B. M.; Chabu, C. Y.; Tesfay, M. Z.; Coleman-Barnett, J.; West, J. T.; Moaven, O. Pancreatic Cancer Tumor Microenvironment is a Major Therapeutic Barrier and Target [Review]. *Front Immunol.* **2024**, *15*, 1287459. 2024. DOI: 10.3389/fimmu.2024.1287459.

[41] Sobczak, M. Enzyme-Responsive Hydrogels as Potential Drug Delivery Systems-State of Knowledge and Future Prospects. *Int. J. Mol. Sci.* **2022**, *23*, 4421. DOI: 10.3390/ijms23084421.

[42] Voo, W.-P.; Ooi, C.-W.; Islam, A.; Tey, B.-T.; Chan, E.-S. Calcium Alginate Hydrogel Beads with High Stiffness and Extended Dissolution Behaviour. *Eur. Polym. J.* **2016**, *75*, 343–353. DOI: 10.1016/j.eurpolymj.2015.12.029.

[43] Malektaj, H.; Drozdov, A. D.; deClaville Christiansen, J. Mechanical Properties of Alginate Hydrogels Cross-Linked with Multivalent Cations. *Polymers (Basel)* **2023**, *15*, 3012. DOI: 10.3390/polym15143012.

[44] Dalheim, M. Ø.; Omtvedt, L. A.; Bjørge, I. M.; Akbarzadeh, A.; Mano, J. F.; Aachmann, F. L.; Strand, B. L. Mechanical Properties of Ca-Saturated Hydrogels with Functionalized Alginate. *Gels* **2019**, *5*, 23. DOI: 10.3390/gels5020023.

[45] Prager, J.; Adams, C. F.; Delaney, A. M.; Chanoit, G.; Tarlton, J. F.; Wong, L.-F.; Chari, D. M.; Granger, N. Stiffness-Matched Biomaterial Implants for Cell Delivery: Clinical, Intraoperative Ultrasound Elastography Provides a 'Target' Stiffness for Hydrogel Synthesis in Spinal Cord Injury. *J. Tissue Eng.* **2020**, *11*, 2041731420934806. DOI: 10.1177/2041731420934806.

[46] Correa, S.; Grosskopf, A. K.; Lopez Hernandez, H.; Chan, D.; Yu, A. C.; Stapleton, L. M.; Appel, E. A. Translational Applications of Hydrogels. *Chem. Rev.* **2021**, *121*, 11385–11457. DOI: 10.1021/acs.chemrev.0c01177.

[47] Mastanamma, S.; Ramkumar, G.; Kumar, D. A.; Rao, J. V. L. N. S. A Stability Indicating RP-HPLC Method for the Estimation of Gemcitabine HCl in Injectable Dosage Forms. *J. Chem.* **2010**, *7*, S239–S244. DOI: 10.1155/2010/724915.

[48] Validation of Analytical Procedures: Text and Methodology. Q2 (R1). 2005;1(20):05.

[49] Lafazanis, K.; Begas, E.; Papapostolou, I.; Iatrou, H.; Sakellaridis, N.; Vlassopoulos, D.; Dimas, K. Development and Validation of a Simple and Reliable HPLC-UV Method for Determining Gemcitabine Levels: Application in Pharmacokinetic Analysis. *Medicina (Kaunas)* **2024**, *60*, 864. DOI: 10.3390/medicina60060864.

[50] Alvarez, I.; Gutiérrez, C.; Gracia, I.; Rodríguez, J. F.; García, M. T. Synthesis of Gemcitabine-Loaded PLGA Microparticles with Green Solvents. *ACS Omega* **2025**, *10*, 33946–33958. DOI: 10.1021/acsomega.5c06385.

[51] Combrzyński, M.; Oniszczuk, T.; Kupryaniuk, K.; Wójtowicz, A.; Mitrus, M.; Milanowski, M.; Soja, J.; Budziak-Wieczorek, I.; Karcz, D.; Kamiński, D.; et al. Physical Properties, Spectroscopic, Microscopic, X-Ray, and Chemometric Analysis of Starch Films Enriched with Selected Functional Additives. *Materials* **2021**, *14*, 2673. DOI: 10.3390/ma14102673.

[52] Henry, B.; Samokhvalov, A. Characterization of Tautomeric Forms of anti-Cancer Drug Gemcitabine and Their Interconversion upon Mechano-Chemical Treatment, Using ATR-FTIR Spectroscopy and Complementary Methods. *J. Pharm. Biomed. Anal.* **2023**, *226*, 115243. DOI: 10.1016/j.jpba.2023.115243.

[53] Prasath, H.; Azhakesan, A.; Manikandan, G. Analytical Methods for Quantification of Gemcitabine in Pharmaceutical and Biological Samples: An Overview of Developments in the Last Decade. 2025.

[54] Ciccolini, J.; Serdjebi, C.; Peters, G. J.; Giovannetti, E. Pharmacokinetics and Pharmacogenetics of Gemcitabine as a Mainstay in Adult and Pediatric Oncology: An EORTC-PAMM Perspective. *Cancer Chemother. Pharmacol.* **2016**, *78*, 1–12. DOI: 10.1007/s00280-016-3003-0.

[55] Gadziński, P.; Froelich, A.; Jadach, B.; Wojtyłko, M.; Tatarek, A.; Białek, A.; Krysztofiak, J.; Gackowski, M.; Otto, F.; Osmałek, T.; et al. Ionotropic Gelation and Chemical Crosslinking as Methods for Fabrication of Modified-Release Gellan Gum-Based Drug Delivery Systems. *Pharmaceutics* **2022**, *15*, 108. DOI: 10.3390/pharmaceutics15010108.

[56] Rakesh, P.; Vipin, K.; Kanchan, K. Alginate Beads Prepared by Ionotropic Gelation Technique: Formulation Design. *Res. J. Chem. Sci.* **2015**, *2231*, 606X.

[57] Patel, N.; Lalwani, D.; Gollmer, S.; Injeti, E.; Sari, Y.; Nesamony, J. Development and Evaluation of a Calcium Alginate Based Oral Ceftriaxone Sodium Formulation. *Prog. Biomater.* **2016**, *5*, 117–133. DOI: 10.1007/s40204-016-0051-9.

[58] Singh, B.; Kaur, T.; Singh, S. Correction of Raw Dissolution Data for Loss of Drug and Volume during Sampling. *Indian J. Pharm. Sci.* **1997**, *59*, 196–199.

[59] Chen, T.-Y.; Tsai, M.-J.; Chang, L.-C.; Wu, P.-C. Co-Delivery of Cisplatin and Gemcitabine via Viscous Nanoemulsion for Potential Synergistic Intravesical Chemotherapy. *Pharmaceutics* **2020**, *12*, 949. DOI: 10.3390/pharmaceutics12100949.

[60] Skwierczynski R, Curry P, Gray V.; et al., editors. Revision of The Dissolution Procedure: Development and Validation< 1092>. *Pharm. Forum*; 2014, Dissolution Technologies.

[61] Vigata, M.; Meinert, C.; Hutmacher, D. W.; Bock, N. Hydrogels as Drug Delivery Systems: A Review of Current Characterization and Evaluation Techniques. *Pharmaceutics* **2020**, *12*, 1188. DOI: 10.3390/pharmaceutics12121188.

[62] Affram, K. O.; Smith, T.; Ofori, E.; Krishnan, S.; Underwood, P.; Trevino, J. G.; Agyare, E. Cytotoxic Effects of Gemcitabine-Loaded Solid Lipid Nanoparticles in Pancreatic Cancer Cells. *J. Drug Deliv. Sci. Technol.* **2020**, *55*, 101374. DOI: 10.1016/j.jddst.2019.101374.